Laboratory synthesis and preparation of thermo-responsive polymeric micelle and hydrogel for resveratrol delivery and release

Zhuojie Zhao[A–D], Liang Xi[B,C], Wei Liang[A–C,E,F]

Department of Orthopedics, The First Affiliated Hospital of Air Force Military Medical University, Xi'an, China

A – research concept and design; B – collection and/or assembly of data; C – data analysis and interpretation;
D – writing the article; E – critical revision of the article; F – final approval of the article

Address for correspondence
Wei Liang
E-mail: liangweiammu@163.com

Abstract

Background. Resveratrol (RSV) exhibits anti-inflammatory, antioxidative, antiaging, and cardioprotective properties. However, due to its hydrophobic nature, it is prone to instability and oxidation, which significantly limit its biomedical applications.

Objectives. The aims of this study were: 1) To prepare and characterize hydrogels and micelles by mixing the synthesized PNIPAM-*b*-PEO-*b*-PNIPAM copolymer and RSV in an aqueous environment; 2) To investigate the molecular interactions between the polymer and RSV; 3) To evaluate various properties of the polymeric micelles and hydrogels; 4) To determine the efficiency of RSV release from the polymeric micelles.

Materials and methods. A well-defined PNIPAM-*b*-PEO-*b*-PNIPAM block copolymer was synthesized and purified. Gel permeation chromatography and ^{1}H NMR were used to characterize the chemical composition and molecular weight of each copolymer. The encapsulation of RSV and its interaction with PNIPAM-*b*-PEO-*b*-PNIPAM were confirmed using 2D nuclear Overhauser effect spectroscopy (NOESY). The lower critical solution temperature (LCST), critical micelle concentration (CMC) and structure of the polymeric micelle were characterized using surface tension measurements, a viscometer, scanning electron microscopy (SEM), and transmission electron microscopy (TEM). The rheological behavior of the RSV-loaded hydrogels was also investigated.

Results. The results showed that the RSV-loaded micelles were successfully prepared. The LCST and CMC of PNIPAM-*b*-PEO-*b*-PNIPAM polymeric micelles were determined to be 35°C and 0.005 g/L, respectively. The micelles have a spherical profile with a particle size of 100 nm and a narrow size distribution.

Conclusions. Resveratrol can be encapsulated within polymeric micelles formed by PNIPAM-*b*-PEO-*b*-PNIPAM block copolymer below the LCST. Its molecules are incorporated into the hydrophobic domains of poly(N-isopropyl acrylamide) (PNIPAM), forming a molecular complex. The point of molecular interaction is primarily at the phenolic region of RSV. Below LCST, PNIPAM-*b*-PEO-*b*-PNIPAM behaves as a polymeric surfactant at low concentrations and as an associating polymer at high concentrations. At high polymer concentrations, PNIPAM-*b*-PEO-*b*-PNIPAM formed a hydrogel. Above LCST, it was released from the polymeric micelles.

Key words: resveratrol, drug release, polymeric micelle

Background

Cartilage regeneration is an important and innovative procedure for replacing damaged knee cartilage.[1–5] Due to the increasing aging population, there is a growing need for cartilage regeneration. Current methods include autologous chondrocyte implantation (ACI).[1] In this method, healthy cartilage cells are taken from the damaged knee and cultured in a lab for several weeks. They are then injected into the damaged joint to regenerate the cartilage along with the surrounding tissue. Although various therapeutic methods have been established, there remains a challenge in achieving cartilage regeneration with normal anatomy, morphology and function. Moreover, repaired cartilage often lacks sufficient mechanical properties, leading to further degeneration. These problems could potentially be solved by the application of hydrogels, which are commonly used as scaffolds for cartilage repair.[6,7]

Resveratrol (RSV, 3,5,4'-trihydroxy-*trans*-stilbene) is a natural phenol found in grape skins, blueberries, raspberries, peanuts, and other plants. It is anti-inflammatory, antioxidative, antiaging, and cardioprotective.[8–11] Importantly, RSV has been reported to suppress the interleukin (IL)-1b-induced inflammatory signaling pathway, making it a promising drug for potential arthritis therapies.[12–15] However, due to its instability under light and heat, as well as its susceptibility to oxidation, the biomedical applications of RSV are limited. Because RSV is a hydrophobic drug, one approach to overcome these challenges is designing an RSV-controlled release system via encapsulation to improve drug administration and therapy efficiency. Encapsulation is considered the most promising way to deliver hydrophobic drugs such as RSV. The primary strategy of encapsulation aims at incorporating a hydrophobic core material into a hydrophilic shell to facilitate the delivery of active agents or drugs into living cells.[16,17] Therefore, an encapsulated system with RSV as the core and biocompatible materials as the shell will not only enhance water solubility of RSV, but also increase its stability by improving photo-stability and resistance against oxidation, thereby enhancing its bioavailability during drug administration.

Stimuli-responsive hydrogel systems are unique due to their high swelling capacity and ability to undergo gelation. These hydrogels can change their appearance or physical properties in response to environmental stimuli such as pH, temperature and light.[18–22] Several thermoresponsive polymers form a gel-like material at temperatures higher than the lower critical solution temperature (LCST).[23–27] Some thermosensitive hydrogels shrink below and dissolve above the upper critical solution temperature (UCST). Typically, thermoresponsive hydrogels consist of a hydrophilic polymer network. Many studies have shown that the gel formation process involves cross-linking of molecular chains through intermolecular interactions (van der Waals forces, hydrophobic interactions, hydrogen bonding, etc.) rather than chemical reactions. A change in ambient temperature can affect these interactions, causing the hydrogel to form in aqueous solution through a simple reversible phase transition (sol–gel). Therefore, the preparation of thermoresponsive hydrogels is straightforward and does not require organic solvents, which is advantageous for delivering hydrophobic drugs. Some studies have shown that thermosensitive poly(N-isopropylacrylamide)-block-poly(ethylene oxide)-block-poly(N-isopropylacrylamide) (PNIPAM-*b*-PEO-*b*-PNIPAM) hydrogels exhibit ideal gel properties, capable of loading protein drugs below 30°C and undergoing a sol–gel phase transition at human body temperature.[23] The PNIPAM-*b*-PEO-*b*-PNIPAM hydrogel has been noted for its good biological degradation and safety.[24–27] However, it still has some unresolved issues such as the need for drug loading at lower temperatures and a short sustained-release cycle (only 7 days) for protein drugs, which limits its clinical application. In addition, an increase in PNIPAM block length can lead to the aggregation of protein drugs.

In this study, a thermosensitive PNIPAM-*b*-PEO-*b*-PNIPAM polymer was synthesized and used as a drug carrier for RSV. Above the LCST, PNIPAM segments become water-insoluble, resulting in the formation of hydrogel with a 3D polymeric network. Hydrophobic junctions within this network, formed by PNIPAM molecules, allow for the loading of RSV molecules. Below the LCST, PNIPAM becomes soluble in aqueous solutions, causing the hydrogel network to collapse and release the RSV molecules. The polymeric structure and incorporation of RSV into PNIPAM junctions were characterized using 2 NMR techniques. Additionally, the critical micelle concentration (CMC) was determined with surface tension. The rheology of PNIPAM-*b*-PEO-*b*-PNIPAM above the overlap concentration (C^*) and the micellar shape, particle size, distribution of the drug within micelles below C^*, and in vitro release properties were investigated.

Objectives

The aim of this study was to design a thermo-induced polymeric hydrogel as a potential carrier for RSV-loaded micelles and injectable hydrogels through: 1) characterizing the chemical structure of the synthesized block copolymer; 2) preparing and characterizing hydrogels and micelles by mixing the synthesized copolymer and RSV in an aqueous environment; 3) investigating the molecular interaction between the polymer and RSV; 4) evaluating various properties of the polymeric micelle and hydrogel; and 5) determining the efficiency of RSV release from the polymeric micelle.

Materials and methods

Materials

Resveratrol (98%) was purchased from Innochem Co Ltd (Beijing, China). The N-isopropyl acrylamide (NIPAM) monomer (M_n~113 g/mol, 98%) and poly(ethylene oxide) (PEO) (M_n~200,000 g/mol) were purchased from Sigma-Aldrich (St. Louis, USA). Ce(IV) ammonium nitrate ($Ce(NO_3)_6(NH_4)_2$) was provided by Wako Pure Chemical Co (Osaka, Japan). All experiments used deionized water obtained from the Millipore-Q water purification system (Merck Millipore, St. Louis, USA). The NIPAM monomer was purified by recrystallization from *n*-hexanes 3 times, while the PEO was purified by dissolving it in dichloromethane and precipitating it in diethyl ether. This purification process was repeated 3 times. Ce(IV) ammonium nitrate was dried at 105°C in a vacuum oven and dissolved in a 1 N aqueous solution of HNO_3 to give a 0.1 M aqueous solution of Ce^{4+} ions. Other chemicals were used as received without further purification.

Synthesis of PNIPAM-*b*-PEO-*b*-PNIPAM

The synthesis procedure was conducted as follows: PEO was dissolved in 20 mL of Milli-Q water in a 200 mL flask and degassed for 2 h under a gentle flow of pure N_2. Ce^{4+} solution was then added to give a Ce^{4+}/PEO molar ratio of 5:1. After stirring this solution for 10 min at 70°C, NIPAM dissolved in 15 mL of Milli-Q water was added under a nitrogen atmosphere. The polymerization was carried out under N_2 at 70°C for 1 h. Upon completion of the polymerization, the solution temperature was reduced to room temperature and dialyzed against Milli-Q water for 3 days using a regenerated cellulose bag with a molecular weight (MW) cutoff of 3,000 g/mol.

The Ce^{4+} and NIPAM solutions were degassed with nitrogen and transferred into the PEO solution using a syringe. Polymerization was carefully conducted to minimize oxygen exposure. Ce^{4+}, NIPAM and PEO solutions were placed in separate round-bottom flasks and degassed for 2 h using nitrogen. The solutions were then transferred with a cannula into the reaction vessel, where polymerization took place. Using high-purity nitrogen from Praxair (Xi'an, China; Ultra High Purity 5.0) improved the polymerization of NIPAM. The synthesis scheme for PNIPAM-*b*-PEO-*b*-PNIPAM is shown in Fig. 1.

The resulting product was dissolved in a 2 M $NaNO_3$ aqueous solution to achieve a 20 wt% solution, which was transferred into an ice bath to ensure complete dissolution. Centrifugation was performed using a Beckman Coulter Avanti J-301 centrifuge (Beckman Coulter, Brea, USA) at 40°C and 8,000 rpm for 60 min. The precipitate was recovered and fully dried with a Labconco Freezone 6 freeze dryer (Labconco, Kansas City, USA) before conducting gel permeation chromatography (GPC) and

NMR analyses. Centrifugation was repeated until GPC and NMR data confirmed the absence of unreacted PEO. Excess salts were removed by dialysis against Milli-Q water for 3 days using a regenerated cellulose bag with an MW cutoff of 3,000 g/mol.

High-resolution ^{1}H NMR spectra of the samples were obtained using a 400 MHz Bruker NMR spectrometer (Bruker, Billerica, USA), with deuterated water (D_2O) as the solvent. The GPC device (Agilent 1260 series; Agilent Technologies, Santa Clara, USA) consisted of a single pump and multi-detector systems, including a light scattering detector, a refractive index detector and a viscosity detector.

Determination of the LCST by turbidimetry, absorbance and viscosity

Turbidimetry measurements were conducted using a DataPhysics MS-20 optical dispersion stability analyzer (DataPhysics Instruments, Filderstadt, Germany) at 0.5°C intervals from 25°C to 40°C. The polymer solution was prepared by dissolving 0.02 g of homopolymer PNIPAM (Sigma-Aldrich; MW = 20,000 g/mol) in 10 mL of Milli-Q water. Absorbance measurements were conducted using the BK4200 UV-vis spectrophotometer (Shanghai Huicheng General Instrument Co., Ltd., Shanghai, China) for a PNIPAM-*b*-PEO-*b*-PNIPAM solution at a concentration of 10 g/L mixed with RSV. The temperature was increased in 0.5°C increments from 25°C to 40°C. Viscosity measurements were conducted using a stress-controlled rheometer (Paar Physica DSR 4000; Anton Paar GmbH, Graz, Austria), with zero-shear viscosity (η_0) used as the viscosity data. The temperature was increased in 0.5°C increments from 25°C to 40°C.

Preparation of RSV-loaded polymeric micelles

Briefly, 0.4 g of PNIPAM-*b*-PEO-*b*-PNIPAM polymer and 0.01 g of RSV were accurately weighed and dissolved in 4 mL and 1 mL of dimethyl formamide (DMF), respectively. After mixing and stirring for 1 h, the solution was loaded into a dialysis bag and dialyzed against 120 L of deionized water for 2 days. The turbid solution obtained from dialysis was centrifuged at 2,000 rpm for 20 min. The supernatant was filtered using a nylon membrane with a pore diameter of 0.15 μm to remove RSV not encapsulated by micelles. The RSV-loaded micelles were obtained by freeze-drying the filtrate.

Characterization of micelle size, profile and structure

The average particle size and distribution of the polymeric micelles were determined using light scattering spectroscopy at 25°C and a wavelength of 486 nm, with
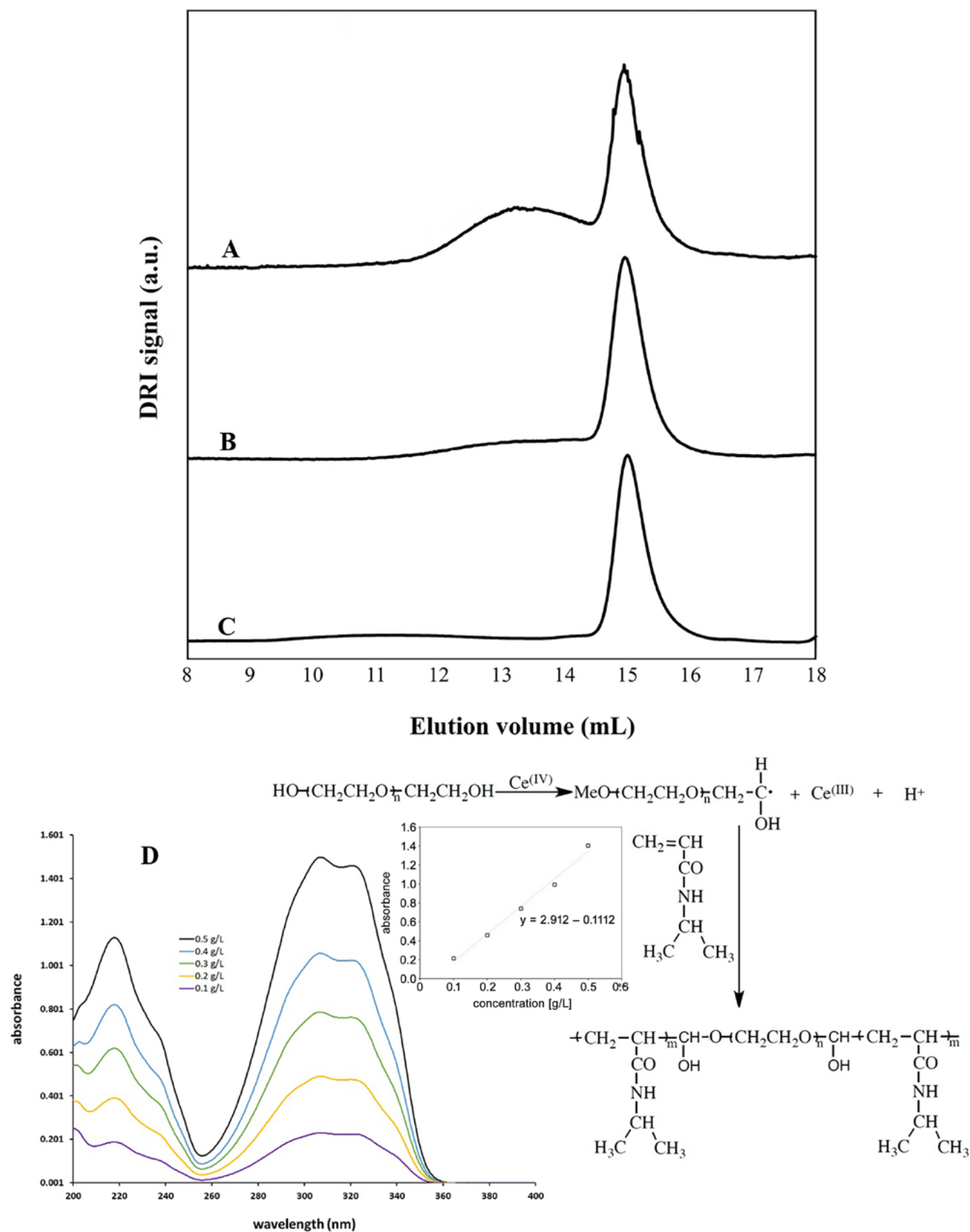
Fig. 1. Top: Synthesis scheme of PNIPAM-*b*-PEO-*b*-PNIPAM. Bottom: gel permeation chromatography (GPC) traces for the crude product synthesis with (A) reactants added through a cannula and using high-purity nitrogen, (B) reactants added through a cannula and degassed with an in-house nitrogen line, and (C) degassed in-house nitrogen; D. UV-vis spectra of samples with various resveratrol (RSV) concentrations and the calibration curve

a scattering angle set to 90°. Transmission electron microscopy (TEM) was used (Hitachi-HT7700; Hitachi Ltd., Tokyo, Japan) to observe the morphology and profile of the micelles. The freeze-dried micelle suspension was dropped onto a copper surface. Phosphotungstic acid (0.1% mass fraction) was used for staining, and the morphology was observed under a lens after drying.

Rheology

Rheological behaviors were investigated using a stress-controlled rheometer (Discovery HR-2; TA Instruments, New Castle, USA) Solutions with viscosities greater than 100 Pa·s were tested using a parallel plate geometry with a 25-mm diameter plate, whereas samples with viscosities below 200 Pa·s were analyzed using a double wall concentric cylinder setup. All experiments were performed at 25 ±2°C. Experimental data were recorded within the range of sensitivity for the rheometer based on the specifications provided by the instrument manufacturer. Angular frequency sweep experiments were conducted under conditions of linear viscoelasticity, where both G' and G'' values remained unchanged with applied stress. The angular frequency interval ranged from 0.01 rad/s to 1,000 rad/s. Various frequency intervals were applied to different sample solutions to ensure that viscoelastic responses were within the sensitivity range of the rheometer, as described in the instrument manual. For the acquisition of viscosity profiles, solutions were subjected to shear with a shear rate ranging from 0.0001 s^{-1} to 100 s^{-1}.

Standard curve of UV spectra of RSV

Resveratrol was dissolved in ethanol to prepare a standard stock solution at a concentration of 0.1 mg/mL. To construct the standard curve, a series of RSV solutions with different concentrations in ethanol were prepared. Ultraviolet–visible (UV-vis) spectra of samples at various RSV concentrations were obtained using a UV-vis spectrophotometer (Shanghai Huicheng General Instrument Co., Ltd.).

Morphology observation

Scanning electron microscopy (SEM) (Hitachi-SU8000; Hitachi Ltd.) and TEM were utilized to observe the morphological structure of polymeric micelles. The solutions were frozen with liquid nitrogen and coated with a thin layer of gold for 60 s at 40 W under vacuum to ensure the electrical conductivity of SEM samples. An excitation voltage of 10 kV was applied for all SEM images.

In vitro release of RSV from polymeric micelles

Two samples (26 mg each) of lyophilized polymeric micelles were accurately weighed and loaded into separate dialysis bags. The lyophilized micelles were dissolved with 5 mL of phosphate-buffered saline (PBS; pH 7.5). Each dialysis bag was sealed and immersed in 25 mL of sodium salicylate solution (1 mol/L) and phosphate buffer (pH 7.5) for an in vitro release experiment conducted in a water bath shaker at 35°C. The solution outside the dialysis bags was replaced with fresh solution of equal volume at set time intervals; the displacement was 10 mL. High-performance liquid chromatography (HPLC) (Agilent Technologies 1260 Infinity; Agilent Technologies, Waldbronn, Germany) was used to detect the content of RSV in the released solution. The cumulative release amount was calculated using Equation 1:

$$E_r\% = \frac{V_e \sum_{i=1}^{n-1} m_i + V_0 m_n}{m_p} \times 100\% \qquad (1)$$

where $E_r\%$ represents the cumulative release amount of RSV in %; V_e is the displacement volume in mL (10 mL); V_0 is the volume of released solution in mL (30 mL); m_i is the mass concentration of RSV at the ith sampling in µg/mL; m_p is the mass of RSV in the loaded polymeric micelles in µg; and n is the displacement number.

Results

Synthesis and characterization of PNIPAM-*b*-PEO-*b*-PNIPAM

Several attempts were made to synthesize PNIPAM-*b*-PEO-*b*-PNIPAM. Initially, the polymerization yielded PNIPAM blocks with a high MW of 12,000 g/mol, albeit with a low overall yield. Although the exact yield was not quantitatively determined, it was qualitatively estimated by examination of the GPC experiments. Depending on the polymerization conditions, the ratio of peak intensity to shoulder decreased, indicating an increase in polymerization yield. Using the high-purity nitrogen, the yield was further increased. After degassing the polymerization vessel with high-purity nitrogen, a significantly higher MW product was obtained, as evidenced by a substantial increase in the signal of crude product. The GPC curves for various attempts are shown in Fig. 1A–C. Analysis of the GPC trace using light scattering and differential refractometer (DRI) detectors revealed a MW of 242,000 g/mol and a polydispersity index (PDI) of 1.43.

The ^{1}H NMR spectrum in Fig. 2A shows assignments for all protons found in the chemical structure of the copolymer sample. Resveratrol was loaded into the polymeric micelle, and the ^{1}H NMR spectrum in Fig. 2B shows the chemical shifts of the protons from the RSV molecule. In contrast, Fig. 2C shows that RSV in D$_2$O without the polymer did not exhibit any peaks because RSV is highly hydrophobic.

To investigate the interaction and incorporation of RSV into PNIPAM hydrophobic junctions below the LCST, 2D nuclear Overhauser effect spectroscopy (NOESY)
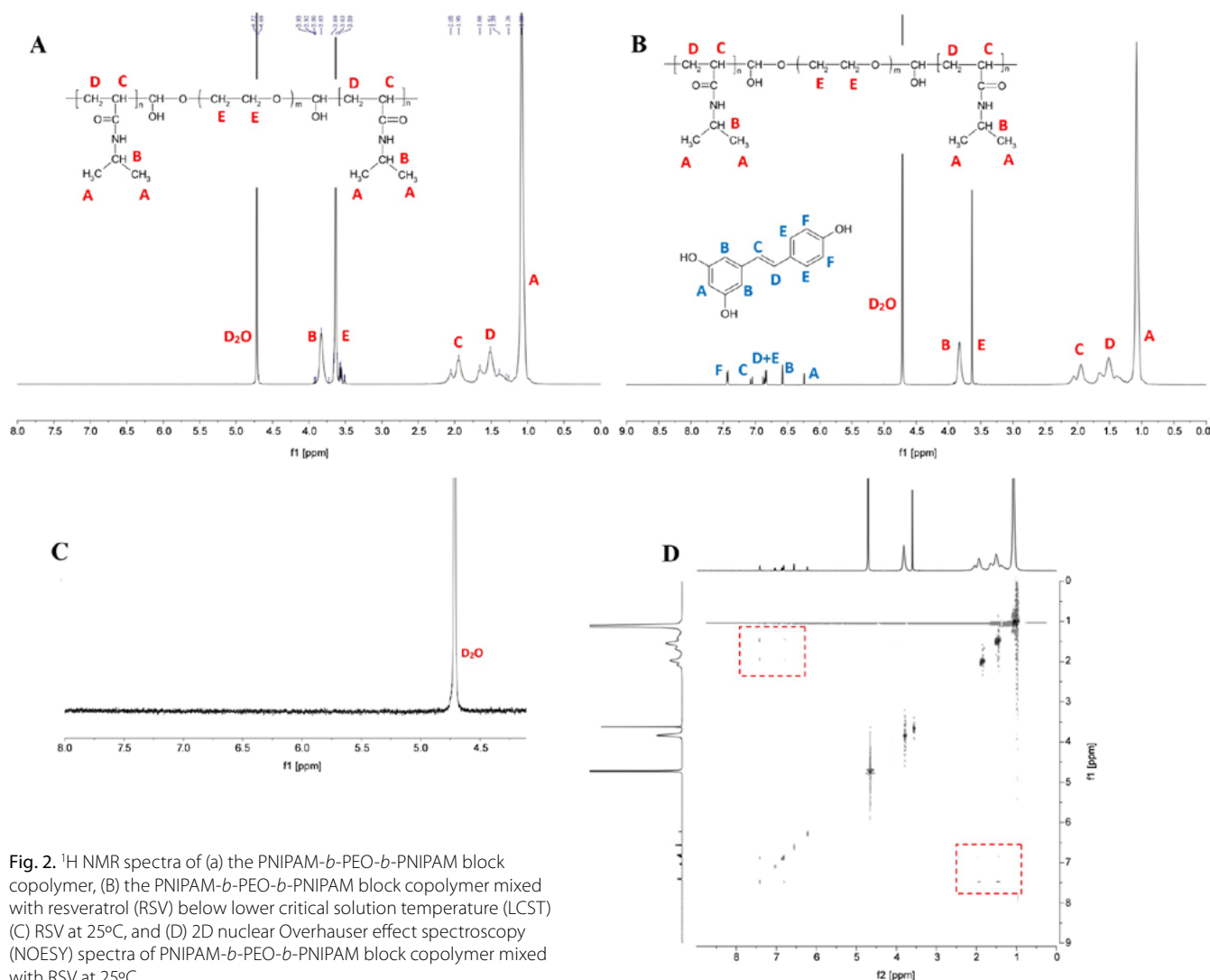
Fig. 2. ¹H NMR spectra of (a) the PNIPAM-*b*-PEO-*b*-PNIPAM block copolymer, (B) the PNIPAM-*b*-PEO-*b*-PNIPAM block copolymer mixed with resveratrol (RSV) below lower critical solution temperature (LCST) (C) RSV at 25ºC, and (D) 2D nuclear Overhauser effect spectroscopy (NOESY) spectra of PNIPAM-*b*-PEO-*b*-PNIPAM block copolymer mixed with RSV at 25ºC

experiments were conducted, and the results are shown in Fig. 2D. In the spectra, there were some signals at the intersections of the peaks from RSV and the PNIPAM blocks, suggesting nuclear Overhauser effect (NOE) or proximity within 0.5 nm between protons of PNIPAM and the RSV molecule. Notably, Fig. 2D also indicates an interaction between the PNIPAM main chain and the RSV aromatic ring bearing 1 hydroxyl group, suggesting that the point of molecular interaction might be at the phenolic part of RSV.

Determination of CMC and *C**

Critical micelle concentration defines the concentration at which a surfactant or polymeric surfactant begins to form micelles. Above CMC, the concentration of free surfactant remains unchanged because additional surfactant molecules will only form more micelles. At CMC, the interface becomes saturated with surfactant molecules, resulting in constant surface tension with increasing surfactant concentration. Figure 3A shows the change in surface tension with increasing polymer concentration

of PNIPAM-*b*-PEO-*b*-PNIPAM at 25°C, with CMC determined to be 45 mg/L from the cross point of 2 fits with different slopes.

At *C**, polymer chains begin to overlap and intermolecular interactions occur. This leads to a sharp increase in solution viscosity due to polymer chain entanglement for water-soluble polymers and hydrophobic association for associating polymers such as PNIPAM-*b*-PEO-*b*-PNIPAM below LCST. Figure 3B shows a plot of viscosity versus polymer concentration of PNIPAM-*b*-PEO-*b*-PNIPAM at 25°C, with *C** determined to be 10.1 g/L from the cross point of 2 fits with different slopes.

Determination of the LCST

The LCST of PNIPAM homopolymer and PNIPAM-*b*-PEO-*b*-PNIPAM block copolymer were determined using a UV-vis spectrophotometer and rheometer. Below the LCST of PNIPAM, the solution remains clear and transmits light at 486 nm with 100% transmission. As the temperature of the solution increases past the LCST
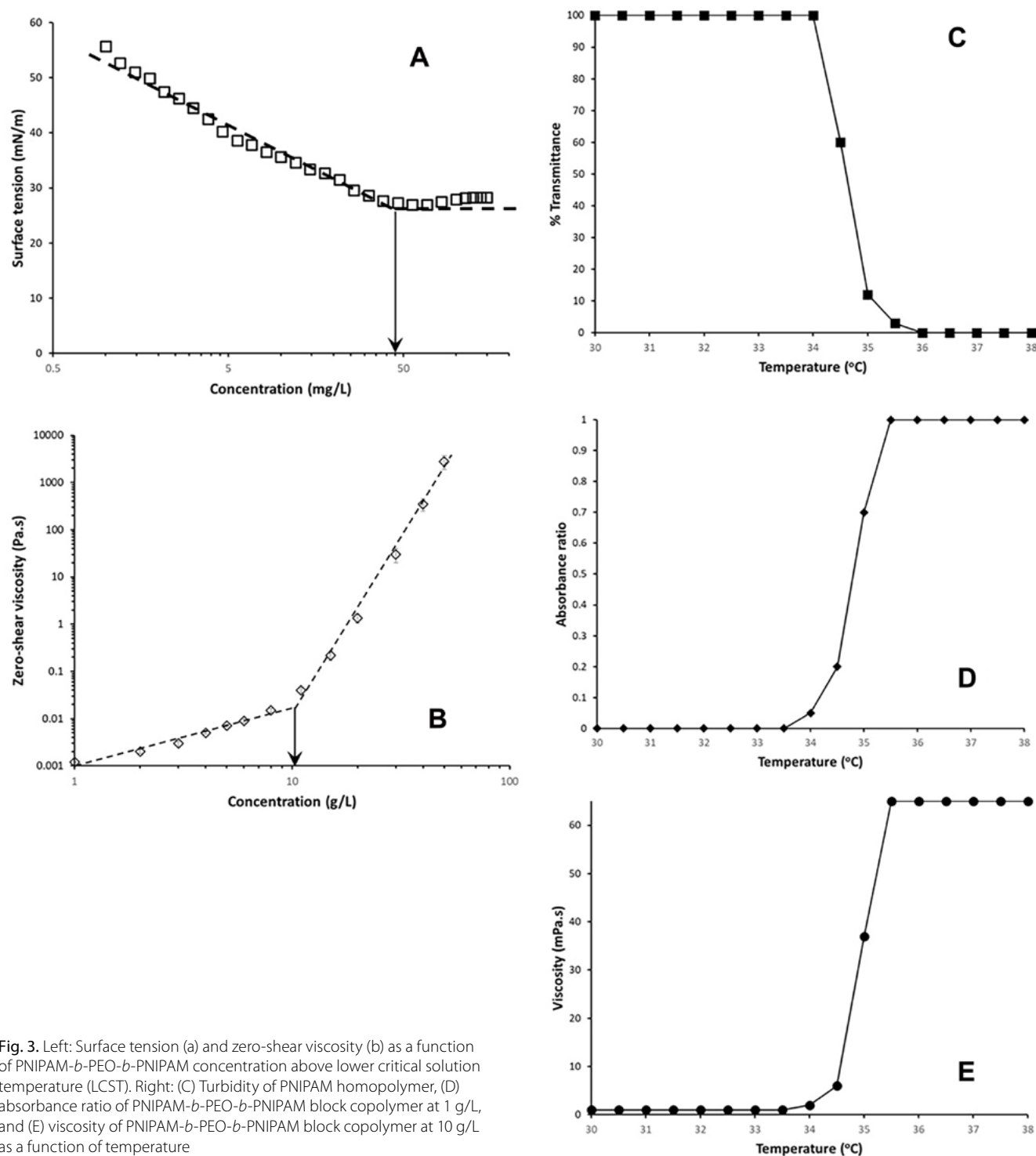
Fig. 3. Left: Surface tension (a) and zero-shear viscosity (b) as a function of PNIPAM-*b*-PEO-*b*-PNIPAM concentration above lower critical solution temperature (LCST). Right: (C) Turbidity of PNIPAM homopolymer, (D) absorbance ratio of PNIPAM-*b*-PEO-*b*-PNIPAM block copolymer at 1 g/L, and (E) viscosity of PNIPAM-*b*-PEO-*b*-PNIPAM block copolymer at 10 g/L as a function of temperature

of PNIPAM, phase separation occurs, the solution becomes turbid, and light transmission drops to 0%. This behavior is illustrated in Fig. 3C for the PNIPAM homopolymer.

For the LCST determination of PNIPAM-*b*-PEO-*b*-PNIPAM, RSV was mixed with the polymer solution at a concentration of 1 g/L. Below the LCST, PNIPAM segments are water-soluble, and hydrophobic RSV is released into the water, resulting in undetectable absorbance in the bulk solution and an absorbance ratio of zero.

Above the LCST, PNIPAM becomes hydrophobic, and RSV dissolves in the hydrophobic core of the polymeric micelle. The absorbance at 307 nm matches that acquired with an equivalent amount of RSV in ethanol, resulting in an absorbance ratio of 1, as shown in Fig. 3D.

At a higher concentration (10 g/L) of PNIPAM-*b*-PEO-*b*-PNIPAM, the entire polymer chain is water-soluble below the LCST (Fig. 3E). Above the LCST, an associating polymer network forms to increase solution viscosity.

Using the above methods, results are presented in Fig. 3C–E. The LCST of PNIPAM-*b*-PEO-*b*-PNIPAM was determined to be 34.5°C, compared to 35°C for PNIPAM homopolymer.

Rheology and viscoelasticity

Figure 4A shows the steady-shear viscosity profiles as a function of shear rate obtained from aqueous solutions of the block copolymer at various concentrations above LCST. A Newtonian region was observed for all samples at lower shear rates, indicating constant viscosity regardless of shear rate. These viscosity values in the regimes are denoted as η_0 and represent the viscosity of the samples under no shear. Figure 4A demonstrates that increasing the block copolymer concentration from 1 g/L to 50 g/L significantly increased the solution viscosity by 10^6-fold, from 1 mPa·s to 2,000 Pa·s. These results suggest that above LCST, the PNIPAM segments become highly hydrophobic, facilitating efficient polymeric network formation through hydrophobic association. Figure 4A also shows that the viscosity significantly decreased, with an increase in shear rate when a shear force was applied to the sample solution. This phenomenon is defined as shear thinning, which is commonly observed in aqueous solutions of hydrophobically modified water-soluble polymers, and it has been widely studied in previous publications. Shear thinning typically results from a transition of inter-molecular hydrophobic associations to intra-molecular associations via the processes of "pull-out" and the rearrangement of hydrophobic units. Figure 4A shows significant shear thinning at lower onset shear rates for samples with higher viscosity, suggesting that this transition occurs more easily in polymer solutions with higher viscosity.

Figure 4B shows the G' and G" results as a function of ω for PNIPAM-*b*-PEO-*b*-PNIPAM block copolymer solutions at various concentrations below LCST. Solutions above 40 g/L exhibited characteristic viscoelastic behavior resembling gels. At a concentration of 50 g/L, the G' and G" values changed only slightly with ω, and all G' values remained higher than G" values, suggesting the dominance of sample elasticity over the sample's viscous flow. Consequently, PNIPAM-*b*-PEO-*b*-PNIPAM at 50 g/L formed a physical gel in water via the hydrophobic association of PNIPAM segments.

Characterization of RSV-loaded polymeric micelles

Dynamic light scattering (DLS) experiments were conducted to measure the particle size distribution of resveratrol (RSV)-loaded polymeric micelles. Figure 5 shows the average diameter of micelles with 6.2% drug loading content (mass fraction). As seen in Fig. 5, the micelle diameter is approx. 100 nm, and the particle size distribution is relatively narrow.
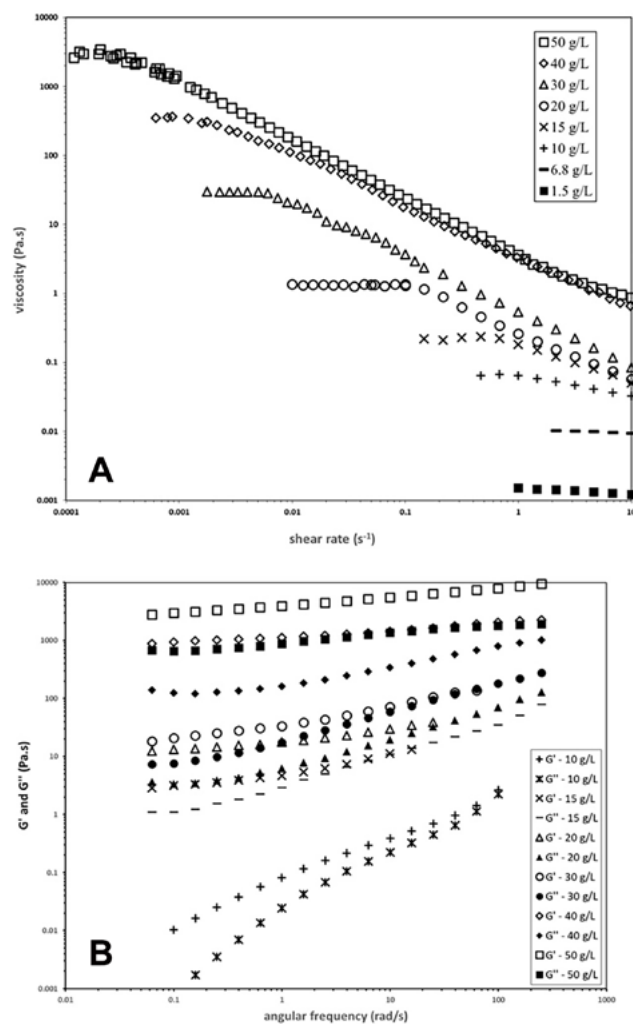

Fig. 4. A. Steady-shear viscosity as a function of shear rate for aqueous solutions of PNIPAM-*b*-PEO-*b*-PNIPAM at various concentrations above lower critical solution temperature (LCST); B. Storage and loss moduli (G' and G") as a function of angular frequency for aqueous solutions of PNIPAM-*b*-PEO-*b*-PNIPAM block copolymer at various concentrations above LCST
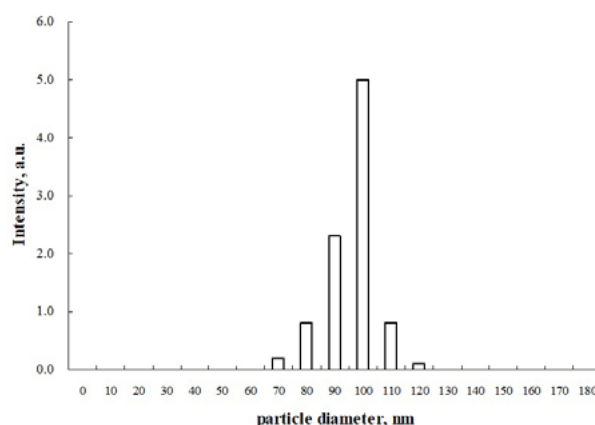

Fig. 5. Particle-size distribution of RSV-loaded polymeric micelles at 25°C

The same method was used to measure the particle size of RSV-loaded micelles with different drug dosages; the obtained data are listed in Table 1. With an increase in RSV

Table 1. The amounts of drug loading and releasing and particle diameter of polymeric micelle with various drug dosage

Drug dosage (by mass fraction, %)	Drug-loading amounts (by mass fraction, %)	Drug-releasing amounts (by mass fraction, %)	Average diameter of polymeric micelles [nm]
6.4	2.9	2.6	101.2
8.7	4.1	3.8	115.6
12.3	5.8	5.2	126.7
16.5	7.6	6.8	266.5

content, the size of polymeric micelles also slightly increased due to more drugs being loaded into the micelles, expanding the hydrophobic core of the polymeric micelle accordingly. At 16.5% RSV content, the micelle size changed significantly, likely due to exposure of a small amount of drugs to the aqueous environment, leading to secondary aggregation of micelles. The encapsulation efficiency of drug-loaded micelles prepared by the dialysis method was low, possibly due to the penetration of a small amount of RSV into the organic solvent from the dialysis bag during dialysis.
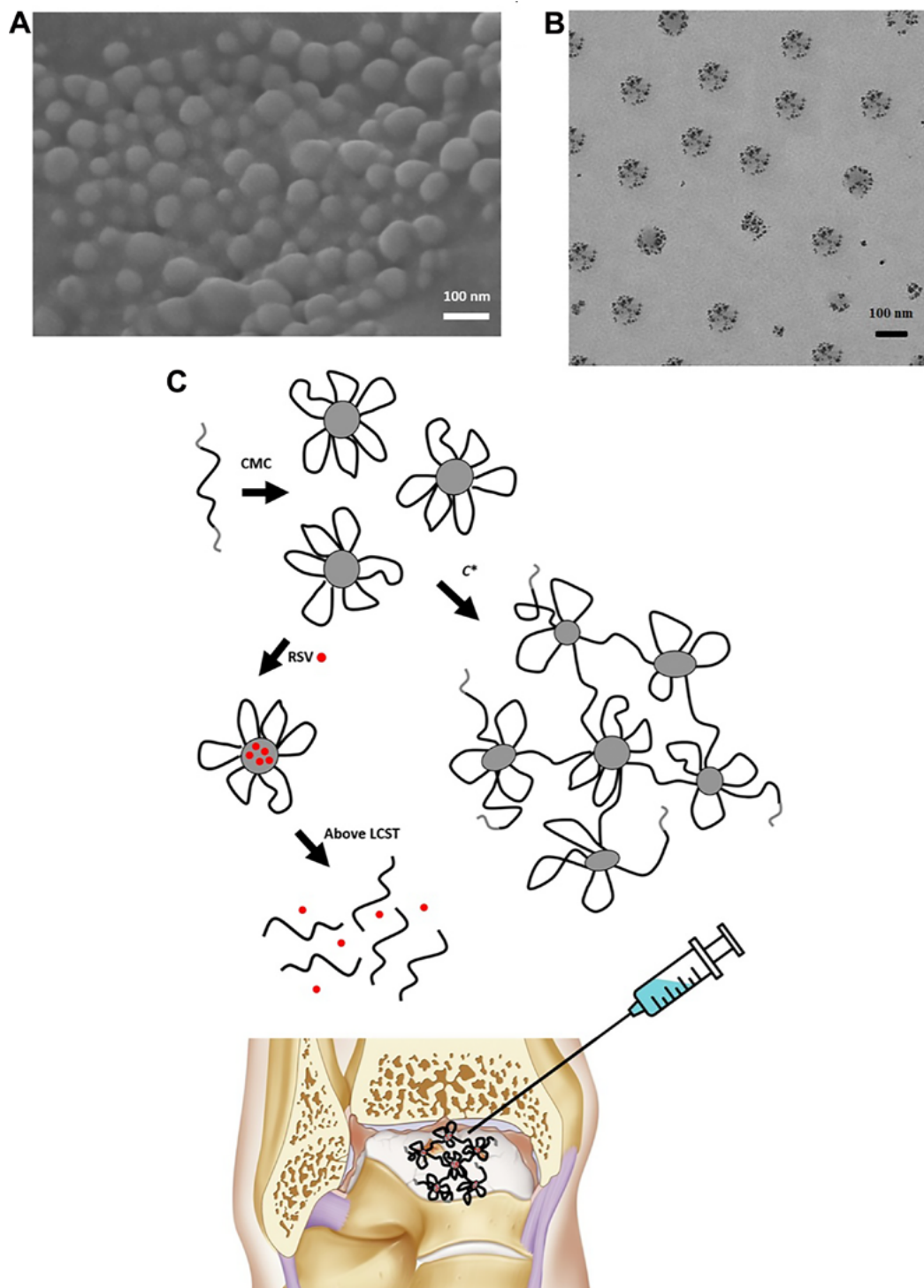
Fig. 6. A. Scanning electron microscopy (SEM) picture of resveratrol (RSV)-loaded polymeric micelles at room temperature; B. Transmission electron microscopy (TEM) picture of RSV-loaded polymeric micelles at room temperature; C. Proposed mechanism for injectable RSV-loaded polymeric micelles or hydrogels for cartilage regeneration

Figure 6A,B presents TEM images of the RSV-loaded polymeric micelles. Generally, the RSV-loaded micelles exhibit a spherical profile with an obvious core-shell structure, and the particle size is relatively uniform (around 100 nm), consistent with the results obtained using the DLS method.

Mechanisms of RSV-loaded polymeric micelles and hydrogel

As shown in Fig. 6C, an injectable RSV delivery system was developed by combining RSV-loaded PNIPAM-*b*-PEO-*b*-PNIPAM copolymer micelles with an in situ forming hydrogel at a high polymer concentration. This approach enhances the stability and retention time of the drug, thereby promoting the performance of cartilage regeneration. Below the CMC of 45 mg/L, the polymer exists as single chains. Above the CMC and the LCST, the PNIPAM blocks become hydrophobic, facilitating the formation of polymeric micelles with hydrophobic domains that accommodate the hydrophobic RSV molecules. As the concentration exceeds $C^* = 10$ g/L, a 3D polymeric network forms, increasing solution viscosity; a physical gel forms above 40 g/L. Below the LCST (34.5°C), the PNIPAM blocks become hydrophilic or water-soluble, causing the collapse of either the micellar structure or the polymeric network, thereby releasing RSV. Given that human body temperature exceeds the LCST of PNIPAM-*b*-PEO-*b*-PNIPAM block copolymers, RSV can be injected in vivo in the form of a hydrogel. Following injection, RSV will target damaged cartilage for repair and regeneration.

Discussion

Resveratrol is a hydrophobic drug. Theoretically, it can be encapsulated into a micellar system in an aqueous environment to establish a controlled release system for delivering RSV to a target site. However, such a system has never been studied or reported for RSV. Previous publications have successfully applied PNIPAM-based hydrogels for the delivery of various drugs, such as levofloxacin,[28] chemokine SDF-1 alpha,[29] melatonin,[30] ciprofloxacin,[31] doxorubicin,[32–34] ibuprofen,[35] and so on. These well-designed PNIPAM-based hydrogel systems have exhibited excellent behavior in drug delivery. Because all of the abovementioned drugs have properties similar to RSV, this study investigated the feasibility of using a PNIPAM and PEO-based hydrogel to deliver RSV. It demonstrated that RSV can be encapsulated into micelles formed by PNIPAM-*b*-PEO-*b*-PNIPAM below the LCST. Structural characterization of the complex indicated the specific position of RSV within the micelle, which is very important for molecular modeling and potential chemical modifications to improve the drug-loading performance. Resveratrol molecules insert themselves into the interior parts

of PNIPAM hydrophobic domains to form a molecular complex. The methyl groups of PNIPAM and the resorcinol part of RSV are not involved in this complex because the aromatic structure is more compact and hydrophobic than linear alkyl chains. The π–π stacking interactions are easily formed between the conjugated structures of the aromatic ring. Polymeric surfactants containing aromatic structures may have a stronger interaction with RSV and could be used to encapsulate more RSV molecules compared to PNIPAM-*b*-PEO-*b*-PNIPAM.

The synthesized copolymer demonstrated a clear LCST. Below this temperature, PNIPAM-*b*-PEO-*b*-PNIPAM behaves like a polymeric surfactant at low concentrations and like an associating polymer at high concentrations. Above 50 g/L, the polymer formed a hydrogel through the hydrophobic association of PNIPAM segments. Resveratrol molecules can be loaded into the hydrogel for in vivo injection. After injection into an environment above the LCST, PNIPAM switches to a hydrophilic state to release the drugs. According to the results presented in Table 1, a large fraction of RSV was released from the polymeric micelle above the LCST, indicating significant potential for RSV delivery and release from this injectable hydrogel formulation.

Limitations

The effectiveness and performance of the RSV-loaded injectable formulation in the current study may be limited by in vitro experiments. Therefore, future studies should include in vivo experiments using experimental animals.

Conclusions

In this study, a thermo-responsive block copolymer consisting of a PEO main chain end-capped with PNIPAM blocks was synthesized for the preparation of RSV-loaded polymeric micelles and injectable hydrogels. The chemical structure of PNIPAM-*b*-PEO-*b*-PNIPAM was confirmed using ^{1}H NMR. The incorporation of RSV into the hydrophobic cores of polymeric micelles was confirmed with 2D NOESY, suggesting that RSV molecules associate with the interior of PNIPAM hydrophobic domains to form the molecular complex. However, the methyl groups of PNIPAM and the resorcinol part of RSV are not involved in this complex. The GPC results yield a polymer with MW of 242,000 g/mol and a PDI of 1.43. The CMC, C^* and LCST of PNIPAM-*b*-PEO-*b*-PNIPAM are 45 mg/L, 10.1 g/L and 34.5°C, respectively. We observed that the PNIPAM-*b*-PEO-*b*-PNIPAM solution exhibits a non-Newtonian plateau at very low shear rates, but at higher shear rates, the viscosity drops dramatically. The polymer at 50 g/L forms a physical gel in water due to the hydrophobic association of PNIPAM segments. The RSV-loaded micelles were successfully prepared; they exhibit a spherical profile and a particle size of 100 nm with a narrow size distribution.

In summary, this RSV-loaded hydrogel system prepared using thermal-responsive copolymers shows potential as an injectable formulation for delivering and releasing RSV for cartilage tissue regeneration.

Data availability

The datasets generated and/or analyzed during the current study are available from the corresponding author on reasonable request.

Consent for publication

Not applicable.

ORCID iDs

Wei Liang https://orcid.org/0009-0002-8374-586X
Zhao Zhuojie https://orcid.org/0009-0007-1786-1113
Liang Xi https://orcid.org/0000-0001-5822-9340

References

1. Behery O, Harris J, Karnes J, Siston R, Flanigan D. Factors influencing the outcome of autologous chondrocyte implantation: A systematic review. *J Knee Surg*. 2012;26(3):203–212. doi:10.1055/s-0032-1329231
2. Marlovits S, Aldrian S, Wondrasch B, et al. Clinical and radiological outcomes 5 years after matrix-induced autologous chondrocyte implantation in patients with symptomatic, traumatic chondral defects. *Am J Sports Med*. 2012;40(10):2273–2280. doi:10.1177/0363546512457008
3. Huey DJ, Hu JC, Athanasiou KA. Unlike bone, cartilage regeneration remains elusive. *Science*. 2012;338(6109):917–921. doi:10.1126/science.1222454
4. Makris EA, Gomoll AH, Malizos KN, Hu JC, Athanasiou KA. Repair and tissue engineering techniques for articular cartilage. *Nat Rev Rheumatol*. 2015;11(1):21–34. doi:10.1038/nrrheum.2014.157
5. Natoli RM, Skaalure S, Bijlani S, Chen KX, Hu J, Athanasiou KA. Intracellular Na$^+$ and Ca^{2+} modulation increases the tensile properties of developing engineered articular cartilage. *Arthritis Rheum*. 2010;62(4):1097–1107. doi:10.1002/art.27313
6. Shi D, Xu X, Ye Y, et al. Photo-cross-linked scaffold with kartogenin-encapsulated nanoparticles for cartilage regeneration. *ACS Nano*. 2016;10(1):1292–1299. doi:10.1021/acsnano.5b06663
7. Roach BL, Kelmendi-Doko A, Balutis EC, Marra KG, Ateshian GA, Hung CT. Dexamethasone release from within engineered cartilage as a chondroprotective strategy against interleukin-1α. *Tissue Eng Part A*. 2016;22(7–8):621–632. doi:10.1089/ten.tea.2016.0018
8. Frischholz S, Berberich O, Böck T, Meffert RH, Blunk T. Resveratrol counteracts IL-1β-mediated impairment of extracellular matrix deposition in 3D articular chondrocyte constructs. *J Tissue Eng Regen Med*. 2020;14(7):897–908. doi:10.1002/term.3031
9. Xing C, Wang Y, Dai X, et al. The protective effects of resveratrol on antioxidant function and the mRNA expression of inflammatory cytokines in the ovaries of hens with fatty liver hemorrhagic syndrome. *Poultry Sci*. 2020;99(2):1019–1027. doi:10.1016/j.psj.2019.10.009
10. Wright C, Krishnan V. Iyer A, Yakisich JS, Azad N. Anti-tumorigenic effects of resveratrol in lung cancer cells through modulation of c-FLIP. *Curr Cancer Drug Targets*. 2017;17(7):669–680. doi:10.2174/1568009617666170315162932
11. Jeong H, Phan AiNH, Choi JW. Anti-cancer effects of polyphenolic compounds in epidermal growth factor receptor tyrosine kinase inhibitor-resistant non-small cell lung cancer. *Pharmacogn Mag*. 2017;13(52):595. doi:10.4103/pm.pm_535_16
12. Wang X, Li X, Duffy P, et al. Resveratrol-loaded poly(D,L-lactide-Co-glycolide) microspheres integrated in a hyaluronic acid injectable hydrogel for cartilage regeneration. *Adv Nanobiomed Res*. 2022;2(1):2100070. doi:10.1002/anbr.202100070
13. Sheu S, Chen W, Sun J, Lin F, Wu T. Biological characterization of oxidized hyaluronic acid/resveratrol hydrogel for cartilage tissue engineering. *J Biomed Mater Res A*. 2013;101(12):3457–3466. doi:10.1002/jbm.a.34653
14. Yu F, Li M, Yuan Z, et al. Mechanism research on a bioactive resveratrol & gelatin porous nano-scaffold in promoting the repair of cartilage defect. *Int J Nanomed*. 2018;13:7845–7858. doi:10.2147/IJN.S181855
15. Wang X, Parvathaneni V, Shukla SK, Kanabar DD, Muth A, Gupta V. Cyclodextrin complexation for enhanced stability and non-invasive pulmonary delivery of resveratrol: Applications in non-small cell lung cancer treatment. *AAPS PharmSciTech*. 2020;21(5):183. doi:10.1208/s12249-020-01724-x
16. Wang J, Shi A, Agyei D, Wang Q. Formulation of water-in-oil-in-water (W/O/W) emulsions containing trans-resveratrol. *RSC Adv*. 2017;7(57):35917–35927. doi:10.1039/C7RA05945K
17. Ansari MJ, Rajendran RR, Mohanto S, et al. Poly(N-isopropylacrylamide)-based hydrogels for biomedical applications: A review of the state-of-the-art. *Gels*. 2022;8(7):454. doi:10.3390/gels8070454
18. Topp MDC, Leunen IH, Dijkstra PJ, Tauer K, Schellenberg C, Feijen J. Quasi-living polymerization of *N*-isopropylacrylamide onto poly (ethylene glycol). *Macromolecules*. 2000;33(14):4986–4988. doi:10.1021/ma9917500
19. Kubota K, Fujishige S, Ando I. Single-chain transition of poly(N-isopropylacrylamide) in water. *J Phys Chem Ref*. 1990;94(12):5154–5158. doi:10.1021/j100375a070
20. Okada Y, Tanaka F. Cooperative hydration, chain collapse, and flat LCST behavior in aqueous poly(*N*-isopropylacrylamide) solutions. *Macromolecules*. 2005;38(10):4465–4471. doi:10.1021/ma0502497
21. Schild HG. Poly(N-isopropylacrylamide): Experiment, theory and application. *Prog Polym Sci*. 1992;17(2):163–249. doi:10.1016/0079-6700(92)90023-R
22. Ono Y, Shikata T. Hydration and dynamic behavior of poly(*N*-isopropylacrylamide)s in aqueous solution: A sharp phase transition at the lower critical solution temperature. *J Am Chem Soc*. 2006;128(31):10030–10031. doi:10.1021/ja063990i
23. Xia Y, Yin X, Burke NAD, Stöver HDH. Thermal response of narrow-disperse poly(*N*-isopropylacrylamide) prepared by atom transfer radical polymerization. *Macromolecules*. 2005;38(14):5937–5943. doi:10.1021/ma050261z
24. Topp MDC, Dijkstra PJ, Talsma H, Feijen J. Thermosensitive micelle-forming block copolymers of poly(ethylene glycol) and poly(*N*-isopropylacrylamide). *Macromolecules*. 1997;30(26):8518–8520. doi:10.1021/ma9710803
25. Motokawa R, Koizumi S, Hashimoto T, Annaka M, Nakahira T. Soap-free emulsion polymerization of poly(ethylene glycol)-*block*-poly(*N*-isopropylacrylamide): Elucidation of specific reaction fields for quasi-living polymerization by time-resolved SANS. *Macromolecules*. 2010;43(2):752–764. doi:10.1021/ma9020533
26. Zhang W, Shi L, Wu K, An Y. Thermoresponsive micellization of poly(ethylene glycol)-*b*-poly(*N*-isopropylacrylamide) in water. *Macromolecules*. 2005;38(13):5743–5747. doi:10.1021/ma0509199
27. Jeon HJ, Go DH, Choi S yee, et al. Synthesis of poly(ethylene oxide)-based thermoresponsive block copolymers by RAFT radical polymerization and their uses for preparation of gold nanoparticles. *Colloids Surf A Physicochem Eng Aspects*. 2008;317(1–3):496–503. doi:10.1016/j.colsurfa.2007.11.033
28. Gan J, Guan X, Zheng J, et al. Biodegradable, thermoresponsive PNIPAM-based hydrogel scaffolds for the sustained release of levofloxacin. *RSC Adv*. 2016;6(39):32967–32978. doi:10.1039/C6RA03045A
29. Yang J, Van Lith R, Baler K, Hoshi RA, Ameer GA. A thermoresponsive biodegradable polymer with intrinsic antioxidant properties. *Biomacromolecules*. 2014;15(11):3942–3952. doi:10.1021/bm5010004
30. Parameswaran-Thankam A, Parnell CM, Watanabe F, et al. Guar-based injectable thermoresponsive hydrogel as a scaffold for bone cell growth and controlled drug delivery. *ACS Omega*. 2018;3(11):15158–15167. doi:10.1021/acsomega.8b01765
31. Liu L, Zeng J, Zhao X, Tian K, Liu P. Independent temperature and pH dual-responsive PMAA/PNIPAM microgels as drug delivery system: Effect of swelling behavior of the core and shell materials in fabrication process. *Colloids Surf A Physicochem Eng Aspects*. 2017;526:48–55. doi:10.1016/j.colsurfa.2016.11.007

32. Giaouzi D, Pispas S. PNIPAM-b-PDMAEA double stimuli responsive copolymers: Effects of composition, end groups and chemical modification on solution self-assembly. *Eur Polym J*. 2020;135:109867. doi:10.1016/j.eurpolymj.2020.109867

33. Ohnsorg ML, Ting JM, Jones SD, Jung S, Bates FS, Reineke TM. Tuning PNIPAm self-assembly and thermoresponse: roles of hydrophobic end-groups and hydrophilic comonomer. *Polym Chem*. 2019;10(25): 3469–3479. doi:10.1039/C9PY00180H

34. Zhang K, Li F, Wu Y, Feng L, Zhang L. Construction of ionic thermo-responsive PNIPAM/γ-PGA/PEG hydrogel as a draw agent for enhanced forward-osmosis desalination. *Desalination*. 2020;495: 114667. doi:10.1016/j.desal.2020.114667

35. Li P, Hou X, Qu L, Dai X, Zhang C. PNIPAM-MAPOSS hybrid hydrogels with excellent swelling behavior and enhanced mechanical performance: Preparation and drug release of 5-fluorouracil. *Polymers (Basel)*. 2018;10(2):137. doi:10.3390/polym10020137